NEON ALGORITHM THEORETICAL BASIS DOCUMENT (ATBD): WATER BAND INDEX (WBI), NORMALIZED MULTI-BAND DROUGHT INDEX (NMDI), NORMALIZED DIFFERENCE WATER INDEX (NDWI), NORMALIZED DIFFERENCE INFRARED INDEX (NDII), AND MOISTURE STRESS INDEX (MSI) ALGORITHM THEORETICAL BASIS DOCUMENT (ATBD)

PREPARED BY	ORGANIZATION	DATE
David Hulslander	AOP	05/29/2019

APPROVALS	ORGANIZATION	APPROVAL DATE
Kate Thibault	SCI	03/28/2022

RELEASED BY	ORGANIZATION	RELEASE DATE
Tanisha Waters	CM	03/28/2022

See configuration management system for approval history.

The National Ecological Observatory Network is a project solely funded by the National Science Foundation and managed under cooperative agreement by Battelle. Any opinions, findings, and conclusions or recommendations expressed in this material are those of the author(s) and do not necessarily reflect the views of the National Science Foundation.

Change Record

REVISION	DATE	ECO #	DESCRIPTION OF CHANGE
A	07/01/2019	ECO-06170	Initial Release
B	03/28/2022	ECO-06794	• Minor formatting updates • Added NEON to document title

TABLE OF CONTENTS

LIST OF TABLES AND FIGURES

1 DESCRIPTION

Contained in this document are details concerning NEON Airborne Imaging Spectrometer (NIS) measurements made at NEON sites. Specifically, the processes necessary to convert "raw" sensor measurements into meaningful scientific units and their associated uncertainties are described.

1.1 Purpose

This document details the algorithms and processes used for creating the NEON Level 2 Canopy Water Content data product, which includes Water Band Index (WBI), Normalized Multi-band Drought Index (NMDI), Normalized Difference Water Index (NDWI), Normalized Difference Infrared Index (NDII), and Moisture Stress Index (MSI) from Level 1 reflectance data. Data Product Identifiers are provided in **Table 1**. Where necessary, this document includes a detailed discussion of appropriate theoretical background, data product provenance, quality assurance and control methods used, approximations and/or assumptions made, and an exposition of uncertainty resulting in a cumulative reported uncertainty for this product.

1.2 Scope

This document describes the theoretical background and entire algorithmic process for creating the NEON Level 2 Canopy Water Content data product (WBI, NMDI, NDWI, NDII, and MSI) from Level 1 reflectance data (RD[03]). It does not provide computational implementation details, except for cases where these stem directly from algorithmic choices explained here.

2 RELATED DOCUMENTS, ACRONYMS AND VARIABLE NOMENCLATURE

2.1 Applicable Documents

AD[01]	NEON.DOC.000001	NEON OBSERVATORY DESIGN
AD[02]	NEON.DOC.002652	NEON Level 1, Level 2 and Level 3 Data Products Catalog
AD[03]	NEON.DOC.002236	AOP Overview Document
AD[04]	NEON.DOC.015015	AOP Payload Integration Mount Design

2.2 Reference Documents

RD[01]	NEON.DOC.000008	NEON Acronym List
RD[02]	NEON.DOC.000243	NEON Glossary of Terms
RD [03]	NEON.DOC.001288	NEON Imaging spectrometer radiance to reflectance algorithm theoretical basis document
RD [04]	NEON.DOC.001290	NEON Algorithm Theoretical Basis Document: Imaging Spectrometer Geolocation Processing
RD [05]	NEON.DOC.001210	NEON Algorithm Theoretical Basis Document: NEON Imaging Spectrometer Level 1B Calibrated Radiance
RD [06]	NEON.DOC.003840	NEON fPAR Algorithm Theoretical Basis Document

2.3 Acronyms

AGL	Above Ground Level
AOP	Airborne Observation Platform
API	Application Programming Interface
ATBD	Algorithm Theoretical Basis Document
ATCOR	Atmospheric Correction
AVIRIS	Airborne Visible/Infrared Imaging Spectrometer
DN	Digital Number
ENVI	Environment For Visualizing Imagery
FPAR	Fraction of Photosynthetically Active Radiation
IDL	Interactive Data Language
IEEE	Institute of Electrical and Electronics Engineers
IFOV	Instantaneous Field Of View
MODIS	Moderate Resolution Imaging Spectroradiometer
MSI	Moisture Stress Index
NCSL	National Conference of Standards Laboratories
NDII	Normalized Difference Infrared Index
NDWI	Normalized Difference Water Index
NEON	National Ecological Observatory Network
NIR	Near Infrared

NIS	NEON Imaging Spectrometer
NMDI	Normalized Multiband Drought Index
NRC	National Research Council
ORNL	Oak Ridge National Laboratory
SWIR	Shortwave Infrared
TOA	Top Of Atmosphere
UTM	Universal Transverse Mercator
VNIR	Visible and Near Infrared
VWC	Vegetation Water Content
WBI	Water Band Index
WGS84	World Geodetic System 1984

3 DATA PRODUCT DESCRIPTION

3.1 Variables Reported

The primary outputs from the NEON Imaging Spectrometer (NIS) WBI, NMDI, NDWI, NDII, and MSI algorithms include:

- WBI raster stored in a GeoTIFF File
- NMDI raster stored in a GeoTIFF File
- NDWI raster stored in a GeoTIFF File
- NDII raster stored in a GeoTIFF File
- MSI raster stored in a GeoTIFF File

The GeoTIFF files contain the output variables as 4-byte floating point pixel data values and use the UTM map projection in the zone appropriate to the site (e.g. UTM 16 N WGS84 for Oak Ridge National Laboratory (ORNL), TN).

3.2 Input Dependencies

A NIS Level 1B reflectance dataset is the only required input for creating the Canopy Water Content (WBI, NMDI, NDWI, NDII, and MSI) data product.

3.3 Product Instances

The NEON data product produced directly from these algorithms is:

Table 1. Data Products generated by Algorithms described in this ATBD.

Data Product Identification Code	Data Product Name
NEON.DOM.SITE.DP2.30019	Canopy Water Content – Spectrometer

3.4 Temporal Resolution and Extent

The NIS Canopy Water Content algorithms are applied on each AOP flight line, which typically measure between 5 and 20 km in length and approximately 600 m in width. Flight speeds are typically around 100 knots (185.2 km/hour), and therefore, the time required to acquire flight lines of the lengths stated will range from 1.6 to 6.5 minutes. The integration time for the NIS detector array is 100 milliseconds, so a time integrated observation is acquired every 100 milliseconds along-track.

NEON sites are planned for varying AOP revisit rates. Most sites have an expected revisit rate of once per year for three of every four years. Some sites, such as those in Domains 20 (Hawaii) and 04 (Puerto Rico), may have less frequent revisits depending upon logistics, budget, and proposal status. Flight schedules are developed for each year on a year-by-year basis in coordination with other NEON

sampling, such as foliar chemistry measurements. Flight schedules are announced at the beginning of each year and are available through the NEON website.

3.5 Spatial Resolution and Extent

The NIS Canopy Water Content algorithms are applied on each AOP flight line, which typically measure between 5 and 20 km in length and approximately 600 m in width, at 1000 m above ground level (AGL). The Instantaneous Field of View (IFOV) of the NEON Imaging Spectrometer is 1.0 milliradian, which equates to a ground sampling distance at a nominal flight of 1000 m AGL of 1 meter at nadir. The actual ground resolution will vary with flight altitude and cross-track field angle. While these variations frequently result in an IFOV which differs from 1 m, NIS data are always resampled to 1 m (RD[04]).

4 SCIENTIFIC CONTEXT

Designed as a decadal- and continental-scale observatory, NEON targets a series of Grand Challenges in the environmental sciences as identified by the National Research Council (NEON, 2011; National Research Council, 2001). Imaging spectrometer data, such as that acquired with the NIS instrument, supports the creation of derived data products which give unique insight in to the types, abundance, and quality of various land covers (Govender et al., 2007). The Grand Challenges include five topics and questions which can be addressed by hyperspectral remote sensing technologies including canopy water content spectral indices:

1. Climate Change
   Carbon-based greenhouse gases such as CO_2 and CH_4 play major roles in driving climate change. The biosphere, including vegetation, is an important part of the carbon cycle. Spectral indices, such as those addressing canopy water content, have shown to be important tools in measuring and mapping the role of the biosphere in the water cycle, carbon cycle, and in climate change for purposes of assessment, modeling, and forecasting (Schlesinger & Bernhardt, 2013).
2. Land Use
   Remote Sensing has a long history in land use mapping, beginning with airborne applications in the early 20th century and with widespread application beginning with the launch of the Earth Resources Technology Satellite in 1972, later renamed to Landsat 1 (Short, 1982). Water indices have been shown to be useful for mapping land cover classes and changes (Jones & Vaughan, 2010).
3. Invasive Species
   Directly mapping invasive vegetation species by spectral signature can be difficult in many cases, or even impossible due to either their differences with native species being too subtle to detect even at higher spatial and spectral resolutions or in cases where they may be understory as compared to native vegetation stands (Jones & Vaughan, 2010). Detecting invasive species using remote sensing is more effectively done by proxies such as plant stress or nutrient cycling/content which are efficiently mapped by spectral indices, including those addressing canopy water content (Clark et al., 1995; Skakun et al., 2003; Coops et al., 2006; Carlson et al., 2007; Borengasser et al., 2008)
4. Biogeochemistry
   Imaging spectrometry, including and especially hyperspectral remote sensing in the VNIR/SWIR spectral range covered by the NIS and similar instruments such as AVIRIS and Hyperion, has been very effective in geochemistry and spectroscopic applications such as material identification and mapping (van der Meer & de Jong, 2011). Canopy water content spectral indices are designed to exploit spectral features specific to water content in vegetation communities and canopies for purposes of assessing their role in the water cycle and climate (Roberts et al., 2016).
5. Biodiversity

While hyperspectral remote sensing can be used for direct species identification given sufficiently high data quality and resolution, canopy water indices can be used as indirect tools for estimating biodiversity in ecological communities (Carlson et al., 2007).

6. Ecohydrology

   Land cover, including vegetation type, density, and health, are important factors in mapping and modeling landscape ecohydrology (Wilcox & Thurow, 2006). How much vegetation covers a landscape, as well as type, vigor, and density, are key factors in run-off, infiltration, nutrient movement, evapotranspiration, and erosion (Scanlon et al., 2005; Foley et al., 1996; Ortenberg, 2012). Canopy water content spectral indices are effective tools and inputs for modeling and characterizing these phenomena and processes (Rodriguez-Iturbe, 2000; Nagler et al., 2007).

4.1 Theory of Measurement

Level 1 NIS hyperspectral reflectance data provide reflectance spectra for each pixel in 426 discrete 5 nm bandpasses for wavelengths from 382 nm to 2512 nm (RD[05]). The unique reflectance spectra of materials on the ground are captured in this data (van der Meer & de Jong, 2011). As full spectral curves and hyperspectral image cubes are difficult and cumbersome to process and analyze, many earth science applications utilize only those spectral regions relevant to the materials or phenomena of interest and their key spectral features (Jones & Vaughan, 2010). This approach also works well with the much broader bandpasses of multispectral sensors (van der Meer & de Jong, 2011). For canopy water content indices, these spectral features and regions include bandpasses at 819, 857, 860, 900, 970, 1241, 1599, 1640, 1649, and 2130 nm (Jones & Vaughan, 2010). The regions are shown in **Figure 1** in the larger context of the electromagnetic spectrum as well as how they relate to the commonly used Landsat 7 and 8 bandpasses.

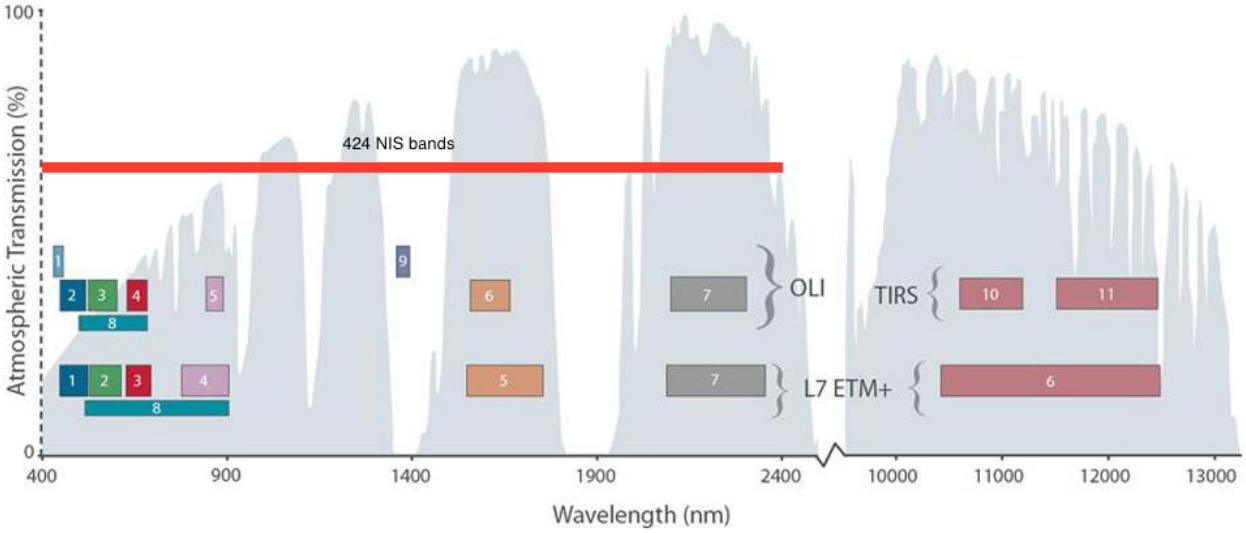

Figure 1. Portions of the electromagnetic spectrum showing % atmospheric transmission and the bandpasses for Landsat 7 (ETM+) and Landsat 8 (OLI and TIRS) sensors. Landsat 8 OLI Bands 2, 3, 4, and 5 correspond to Blue, Green, Red and Near Infrared (NIR), respectively. Landsat has used 4 to 9 bands, depending on generation, to cover the roughly 400 to 2400 nm portion of the spectrum here, which is covered by the NEON Imaging Spectrometer with 424 5-nm-wide bands. (USGS, 2013).

For spectral indices, the reflectance values of the spectral bandpasses of interest are combined using various functions, often as normalized ratios of two or more bands. This reduces the data volume to a single value per pixel directly related to the topic of study and comparable across both space and time and even between different sensors and datasets. As ratios are inherently relative measures, using them can help reduce the error common to the absolute measure of the bands involved. Many such indices are now common in remote sensing earth science applications, including but not limited to (Thenkabail et al, 2012):

- Water Band Index (WBI)
- Normalized Multi-band Drought Index (NMDI)
- Normalized Difference Water Index (NDWI)
- Normalized Difference Infrared Index (NDII)
- Moisture Stress Index (MSI)

4.2 Theory of Algorithm

Though they differ in the phenomenology on which they focus, all canopy water content spectral indices have the same basic approach of using two to three spectral bands related to reflectance or absorption by water as it is found in vegetation communities and canopies and combining those bands in unitless ratios. The following subsections, one per index covered in this document, detail the theory behind each index's particular ratio algorithm. Currently, NIS bands are selected to most closely match the center of historically used broader multispectral ranges or most closely match the specified band(s) for the index as specified in the index's original publication as noted.

4.2.1 Water Band Index (WBI)

Penuelas et al (1993) derived the Water Band Index, targeting the 970 nm water absorption band and a reference band at 900 nm. Their study, using beans and peppers, found it to be a good proxy for relative water content and plant water status in agricultural crops without bare soil. The study also showed WBI to have good sensitivity when plant water stress was well developed. As a result, it may be of most use for agricultural management and assessment, fire hazard assessment, and water cycle modeling and analysis. The ideal WBI algorithm is given in Eq. 1.

$$WBI = \frac{\rho_{970}}{\rho_{900}} \quad \textbf{Eq. 1}$$

4.2.2 Normalized Multi-band Drought Index (NMDI)

NMDI is a broadband spectral index derived and proposed by Wang and Qu (2007) and originally intended for use with data from orbital sensors such as MODIS for remotely sensing both soil and vegetation water content. Their study showed NMDI has enhanced sensitivity to drought severity compared to NDWI and NDII. While their study indicated NMDI is useful for water content estimation in relatively pure soil and vegetation pixels, it could yield inaccurate results in mixed pixels with LAI between 0.5 and 1.0. In combination with its sensitivity to both soil and vegetation moisture content, NMDI has possible applications in fire hazard assessment and water cycle studies (Wang et al., 2008). The ideal NMDI algorithm is given in Eq. 2.

$$NMDI = \frac{\rho_{860} - (\rho_{1640} - \rho_{2130})}{\rho_{860} + (\rho_{1640} - \rho_{2130})} \quad \textbf{Eq. 2}$$

4.2.3 Normalized Difference Water Index (NDWI)

First proposed by Gao (1996), the NDWI is designed as a narrowband hyperspectral index for remotely sensing liquid water in vegetation from orbital sensors. Similar in formulation to NDVI, Gao found NDWI to exhibit similar sensitivities to in-pixel bare soil contributions but as NDVI saturated at higher vegetation water content values and multiple layers of leaves, NDWI continued to vary with VWC. Jackson et al (2004) found similar results and were able to show NDWI-derived VWC compared to ground measurements for soybeans and corn had lower bias (-0.015 and -0.010 respectively) and RMSE (0.171 and 0.576) than NDVI-derived VWC (biases of 0.071 and 0.336, RMSE values of 0.203 and 0.735). NDWI is often considered to be a vegetation index as well as a canopy water index and has been useful in multispectral (Landsat) vegetation water content mapping for agricultural, fire hazard assessment, and water cycle analysis and modeling (Jackson et al., 2003).

$$NDWI = \frac{(\rho_{857} - \rho_{1241})}{(\rho_{857} + \rho_{1241})} \quad \textbf{Eq. 3}$$

4.2.4 Normalized Difference Infrared Index (NDII)

First developed and used as a multispectral radiance index, NDII is useful for applications in mapping vegetation canopy water content (Hardisky et al., 1983). Sriwongsitanon et al (2015) showed good results using NDII in agricultural and forestry applications, especially when addressing soil moisture storage during the dry season, obtaining average R^2 values of 0.87. For fire hazard applications, Chuvieco et al. (2002) found good results in grassland and shrubland ecosystems, while Dasgupta et al. (2007) had poorer results in forests.

$$NDII = \frac{(\rho_{819} - \rho_{1649})}{(\rho_{819} + \rho_{1649})}$$ **Eq. 4**

4.2.5 Moisture Stress Index (MSI)

First developed and used with Landsat data for assessing leaf water content, MSI has also been useful for applications in monitoring and detecting forest damage, and relative water content mapping (Rock et al., 1985; Rock et al., 1986; Hunt & Rock, 1989). These strengths, combined with the possibility of using widely available broadband multispectral data, make MSI a popular tool in climate change, land use, invasive species, forestry, agriculture, and ecohydrological applications.

$$MSI = \frac{\rho_{1599}}{\rho_{819}}$$ **Eq. 5**

4.3 Special Considerations

While the equations for these indices are well settled and agreed upon, the exact wavelength ranges or bandpasses to be used in each are largely undetermined. Most canopy water content spectral index products are constrained to the larger bandpasses of the multispectral instruments for which they are developed, e.g. Landsat and MODIS "blue", "red", and "NIR" bands. Historically, researchers using hyperspectral instruments such as AVIRIS have chosen either single bands closest to the band centers of the popular multispectral bandpasses mentioned above, or have used a weighted resampling of a number of the hyperspectral bands to mimic the broader multispectral bandpasses (Vane, 1988).

The NIS instrument, however, provides a new level of flexibility in choosing which spectral bands to choose in calculating band indices and ratios. Where a multispectral sensor may offer one band for "NIR", NIS will offer a selection from one to tens of bands that may be used, excluded, or combined in various ways.

For current implementation of canopy water content spectral index products, NEON will be using single NIS bands closest to the band centers of the relevant traditional multispectral bands. In 2018, NEON will be optimizing the combination of NIS channels in production implementation of these indices. The combination of channels will be chosen to best capture the spectral features required for each index.

5 ALGORITHM IMPLEMENTATION

The processing of the NIS reflectance data to the canopy water content spectral indices data is achieved in the steps shown in the left column of **Figure 2**. The NIS canopy water content spectral index algorithms have been implemented in IDL and use the ENVI API for data access and processing.

Inputs: NEON Imaging Spectrometer L1 Orthorectified Surface Directional Reflectance data product (NEON.DOM.SITE.DP1.30006).

As each of the three NIS instruments is individually manufactured, exact spectral bandpasses between the instruments are not identical. To maximize compatibility of vegetation index products across the sensors in initial vegetation index algorithm implementation, the bands used for calculating the indices are currently chosen to be those closest to the centers as defined in the literature. The desired band centers used for the indices are shown in **Table 2**. As described in Section 8, the vegetation index algorithm implementation will be upgraded in 2018 to use specified bandpasses centered on the desired band centers for each variable in the vegetation indices and input sensor bands will be convolved to those bandpasses.

Table 2. Water indices, their optimal center wavelengths, and their references.

Water Index	Band centers used in index (nm)	Reference
WBI	900, 970	Penuelas et al., 1993
NMDI	860, 1640, 2130	Wang & Qu, 2007
NDWI	857, 1241	Gao, 1996
NDII	819, 1649	Hardisky et al., 1983
MSI	819, 1599	Rock et al., 1985

6 UNCERTAINTY

As the canopy water content index products described in this document are all entirely derived from L1 NIS surface reflectance data combined in normalized ratios, their uncertainties are therefore entirely dependent on the uncertainty in the L1 reflectance data and the combinations and ratios of bands used in each index. Additional sources of errors or uncertainties will be included in analysis as they are identified during the course of observatory construction and operation. There are a number of sources of uncertainty contributing to the reflectance data product uncertainty, as shown in **Figure 2**. The detailed analysis of uncertainty in the reflectance data is discussed in the L1 Reflectance ATBD. The reported uncertainty values from the L1 Reflectance ATBD are used here. A summary of them is in **Table 3**.

Table 3. Summary of expected reflectance uncertainties due to site and observing conditions, data acquisition procedures, instrumentation nature, and data processing requirements.

Data Quality	Surface Type	Atmospheric Conditions	ρ Error (% reflectance)
Ideal	Well characterized, low complexity	Well characterized, spatially and temporally consistent, clear	± 2%
Medium	Moderately complex, moderately well characterized	Some spatial and temporal variation, moderate haze and aerosol	± 5%
Low	Highly complex and/or poorly characterized	Poorly characterized, highly variable, anomalous conditions	± 10%

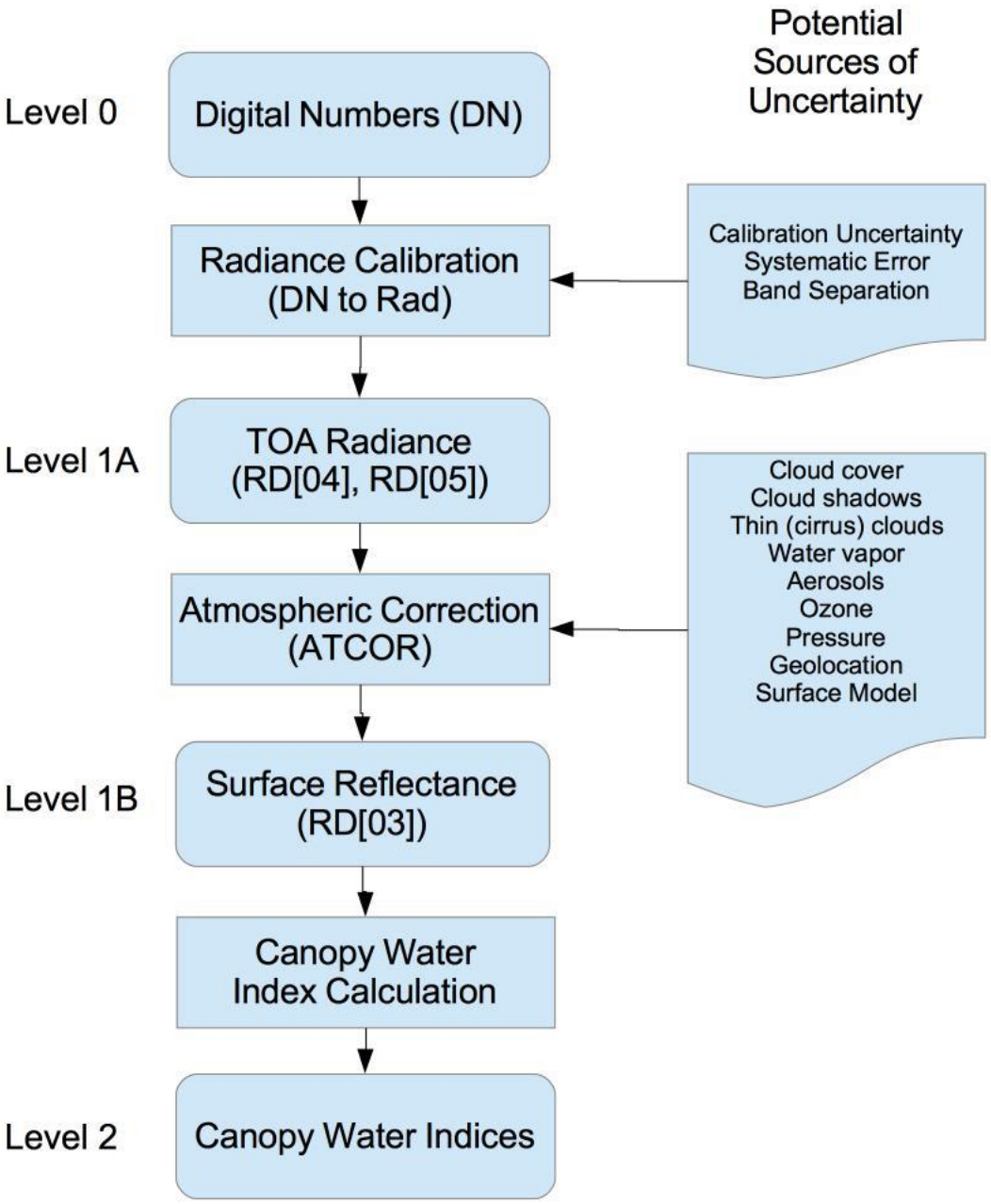

Figure 2. End-to-end canopy water content spectral index processing chain diagram including sources of uncertainty in upstream processing and systems contributing to the reflectance data input required for calculating canopy water content spectral indices.

6.1 Analysis of Uncertainty

Propagation and accumulation of uncertainty from sources in to the canopy water content spectral index products can be modeled using the "law of propagation of uncertainty" (NCSL, 1997; Taylor & Kuyatt, 1994). This approach handles only random errors, does not consider systematic biases, and assumes statistical independence in the errors. Systematic errors and biases are addressed in the processing of the raw NIS data to the surface reflectance values used here (RD[03], RD[04], RD[05]). As has been done with MODIS vegetation indices, we use the framework of water indices being a quantity of interest *y* based on a function combining estimates of *n* other quantities as shown in Eq. 6 (Huete et al., 1999).

$$y = f(x_1, x_2, \ldots, x_n) \quad \textbf{Eq. 6}$$

An uncertainty propagation equation, Eq. 7, can be based on a first-order Taylor series expansion of Eq. 6, where *u* is uncertainty (Huete et al., 1999).

$$u^2 = \sum_{i=1}^{n}\sum_{j=1}^{n} \frac{\partial f}{\partial x_i}\frac{\partial f}{\partial x_j} u(x_i, x_j) = \sum_{i=1}^{n}\left(\frac{\partial f}{\partial x_i}\right)^2 u^2(x_i) + 2\sum_{i=1}^{n-1}\sum_{j=i+1}^{n} \frac{\partial f}{\partial x_i}\frac{\partial f}{\partial x_j} u(x_i, x_j) \quad \textbf{Eq. 7}$$

From Eq. 7 a set of uncertainty propagation equations designed for reflectance calibration uncertainties in atmospherically corrected canopy water content spectral indices can be created and are shown in their respective sections below (Miura et al., 1999). From those equations, it can be seen that error in the indices will vary with both the error of the input reflectance and with the actual reflectance values. Uncertainty estimations for surface reflectance values have been developed during AOP construction and will be rigorously monitored and revised during operations via lab and field calibration and validation activities.

In each of the following subsections, uncertainty values are calculated across the range of all possible combinations of input reflectance values and the results presented as surfaces. Some of these surfaces show certain combinations of reflectance values can result in uncertainty increasing very rapidly. The combinations of values that result in uncertainty rising asymptotically are where two or more of the bands have reflectance values approaching 0.0 or 1.0. While this is theoretically possible, e.g. extremely dark shadows or extremely bright surfaces, it is very unlikely in real world data or practical use cases and would occur only over areas where vegetation indices would be inappropriate or not useful.

6.1.1 WBI Uncertainty

Because WBI is a simple two-band ratio, as shown earlier in Eq. 1, WBI can theoretically range from zero to infinity. The equation for WBI uncertainty as derived from Eq. 7 is shown in Eq. 8 (Huete et al., 1999).

$$u_{cal}^2(WBI) = \left(\frac{\partial WBI}{\partial \rho_{970}}\right)^2 u_{cal}^2(\rho_{970}) + \left(\frac{\partial WBI}{\partial \rho_{900}}\right)^2 u_{cal}^2(\rho_{900}) + 2\frac{\partial WBI}{\partial \rho_{970}}\frac{\partial WBI}{\partial \rho_{900}} u_{cal}(\rho_{970}, \rho_{900})$$

Eq. 8

where

$$\frac{\partial WBI}{\partial \rho_{970}} = \frac{1}{\rho_{900}}$$

Eq. 9

$$\frac{\partial WBI}{\partial \rho_{900}} = -\frac{\rho_{970}}{{\rho_{900}}^2}$$

Eq. 10

$$\frac{\partial WBI}{\partial \rho_{970}}\frac{\partial WBI}{\partial \rho_{900}} = -\frac{\rho_{970}}{{\rho_{900}}^3}$$

Eq. 11

Error in WBI has been calculated for all combinations of ρ_{970} and ρ_{900} reflectance values from 5% to 95% for 2%, 5%, and 10% error in those values. The surface plot for the 5% error calculations are in **Figure 3**.

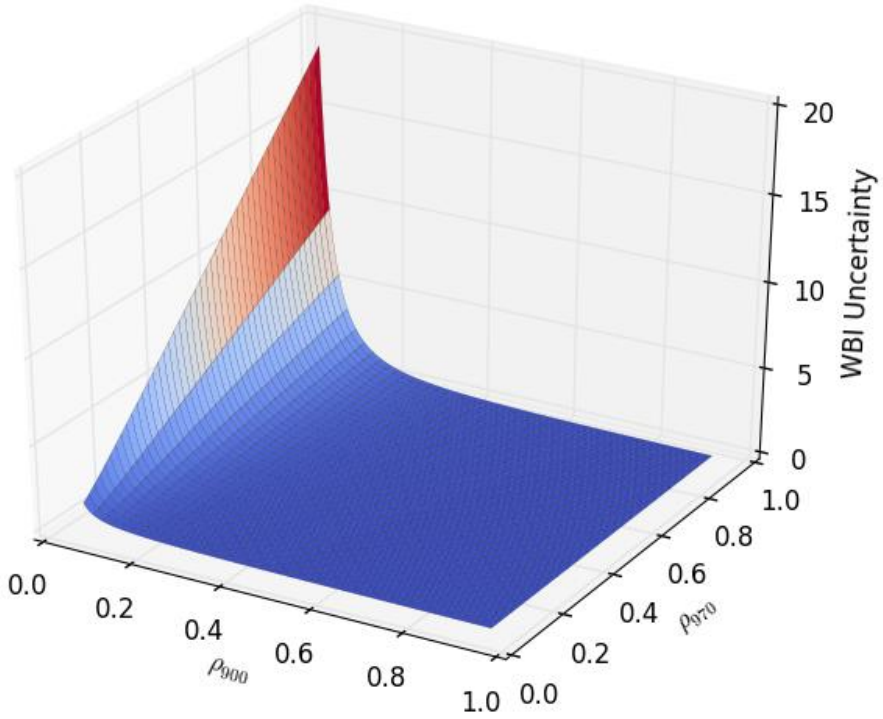

Figure 3. Error in WBI as a function of input reflectance values with 5% uncertainty. Error surfaces for WBI with different reflectance value uncertainty retain the same shape and differ only by magnitude.

6.1.2 NMDI Uncertainty

Because NMDI is a ratio of three bands, as shown earlier in Eq. 2, NMDI uncertainty varies across the full range of NMDI values. The equation for NMDI uncertainty as derived from Eq. 7 is show in Eq. 12 (Huete et al., 1999).

$$u_{cal}^2(NMDI) = \left(\frac{\partial NMDI}{\partial \rho_{860}}\right)^2 u_{cal}^2(\rho_{860}) + \left(\frac{\partial NMDI}{\partial \rho_{1640}}\right)^2 u_{cal}^2(\rho_{1640}) + \left(\frac{\partial NMDI}{\partial \rho_{2130}}\right)^2 u_{cal}^2(\rho_{2130}) + 2\frac{\partial NMDI}{\partial \rho_{860}}\frac{\partial NMDI}{\partial \rho_{1640}} u_{cal}(\rho_{860},\rho_{1640}) + 2\frac{\partial NMDI}{\partial \rho_{860}}\frac{\partial NMDI}{\partial \rho_{2130}} u_{cal}(\rho_{860},\rho_{2130}) + 2\frac{\partial NMDI}{\partial \rho_{1640}}\frac{\partial NMDI}{\partial \rho_{2130}} u_{cal}(\rho_{1640},\rho_{2130}) \quad \textbf{Eq. 12}$$

where

$$\frac{\partial NMDI}{\partial \rho_{860}} = \frac{2(\rho_{1640} - \rho_{2130})}{(\rho_{860} + (\rho_{1640} - \rho_{2130}))^2} \quad \textbf{Eq. 13}$$

$$\frac{\partial NMDI}{\partial \rho_{1640}} = \frac{-2\rho_{860}}{(\rho_{860} + (\rho_{1640} - \rho_{2130}))^2} \quad \textbf{Eq. 14}$$

$$\frac{\partial NMDI}{\partial \rho_{2130}} = \frac{2\rho_{860}}{(\rho_{860} + (\rho_{1640} - \rho_{2130}))^2} \quad \textbf{Eq. 15}$$

Error in NMDI has been calculated for all combinations of ρ_{860} and ρ_{1640} reflectance values from 5% to 95% for 2%, 5%, and 10% error in those values with the ρ_{1640} reflectance fixed at 5% with uncertainty values equal to those for ρ_{860} and ρ_{1640}. As ρ_{1640} increases there are many points where input reflectance values can combine such that NMDI becomes undefined due to the construction of its denominator. The surface plot for the 5% error calculations are in **Figure 4**.

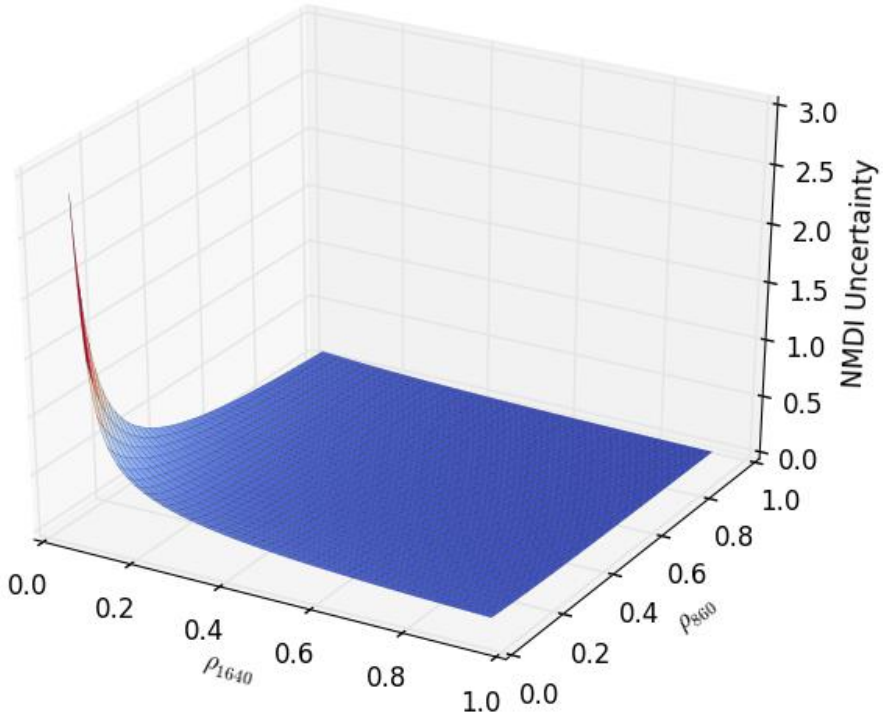

Figure 4. Error in NMDI as a function of varying ρ_{860} and ρ_{1640} reflectance values, ρ_{2130} reflectance of 5%, and all reflectance values with 5% uncertainty. Error surfaces for NMDI with different reflectance value uncertainty retain the same shape and differ only by magnitude.

6.1.3 NDWI Uncertainty

Because NDWI is a normalized ratio of two bands, as shown earlier in Eq. 3, NDWI uncertainty varies across the allowed range of NDWI from -1 to 1. The equation for NDWI uncertainty as derived from Eq. 7 is show in Eq. 16 (Huete et al., 1999).

$$u_{cal}^2(NDWI) = \left(\frac{\partial NDWI}{\partial \rho_{857}}\right)^2 u_{cal}^2(\rho_{857}) + \left(\frac{\partial NDWI}{\partial \rho_{1241}}\right)^2 u_{cal}^2(\rho_{1241}) + 2\frac{\partial NDWI}{\partial \rho_{857}}\frac{\partial NDWI}{\partial \rho_{1241}} u_{cal}(\rho_{857},\rho_{1241}) \quad \textbf{Eq. 16}$$

where

$$\frac{\partial NDWI}{\partial \rho_{857}} = \frac{2\rho_{1241}}{(\rho_{857} + \rho_{1241})^2}$$

Eq. 17

$$\frac{\partial NDWI}{\partial \rho_{1241}} = \frac{-2\rho_{857}}{(\rho_{857} + \rho_{1241})^2}$$

Eq. 18

$$\frac{\partial NDWI}{\partial \rho_{857}} \frac{\partial NDWI}{\partial \rho_{1241}} = \frac{-4\rho_{857}\rho_{1241}}{(\rho_{857} + \rho_{1241})^4}$$

Eq. 19

Error in NDWI has been calculated for all combinations of ρ_{857} and ρ_{1241} reflectance values from 5% to 95% for 2%, 5%, and 10% error in those values. The surface plot for the 5% error calculations are in **Figure 5**.

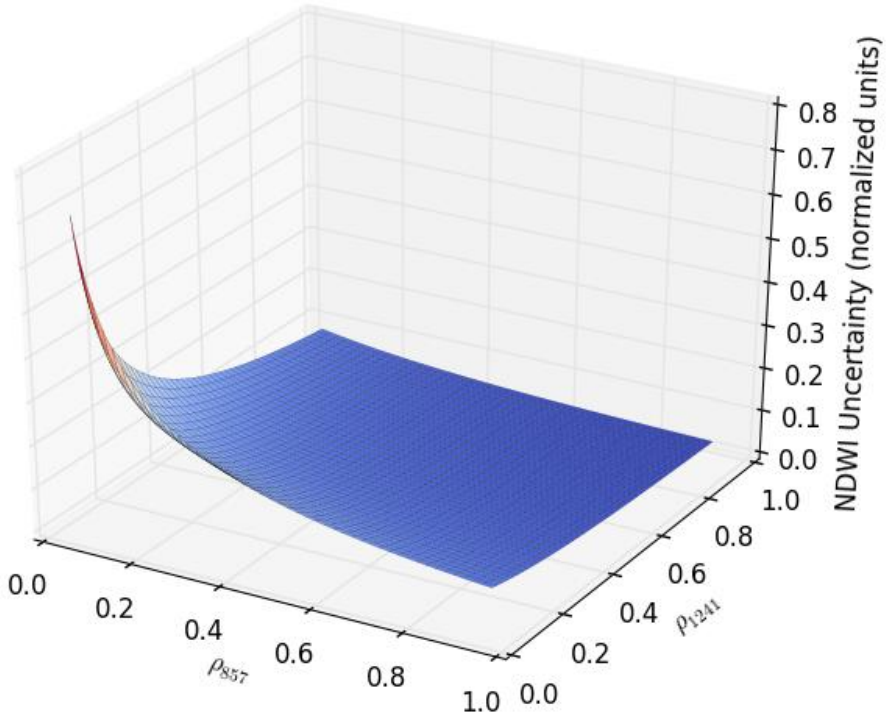

Figure 5. Error in NDWI as a function input reflectance values with 5% uncertainty. Error surfaces for NDWI with different reflectance value uncertainty retain the same shape and differ only by magnitude.

6.1.4 NDII Uncertainty

Because NDII is a normalized ratio of two bands, as shown earlier in Eq. 4, NDII uncertainty varies across the allowed range of NDII from -1 to 1. The equation for NDII uncertainty as derived from Eq. 7 is shown in Eq. 20 (Huete et al., 1999).

$$u_{cal}^2(NDII) = \left(\frac{\partial NDII}{\partial \rho_{819}}\right)^2 u_{cal}^2(\rho_{819}) + \left(\frac{\partial NDII}{\partial \rho_{1649}}\right)^2 u_{cal}^2(\rho_{1649}) + 2\frac{\partial NDII}{\partial \rho_{819}}\frac{\partial NDII}{\partial \rho_{1649}} u_{cal}(\rho_{819},\rho_{1649}) \quad \textbf{Eq. 20}$$

where

$$\frac{\partial NDII}{\partial \rho_{819}} = \frac{2\rho_{1649}}{(\rho_{819} + \rho_{1649})^2}$$

Eq. 21

$$\frac{\partial NDII}{\partial \rho_{1649}} = \frac{-2\rho_{819}}{(\rho_{819} + \rho_{1649})^2}$$

Eq. 22

$$\frac{\partial NDII}{\partial \rho_{819}} \frac{\partial NDII}{\partial \rho_{1649}} = \frac{-4\rho_{819}\rho_{1649}}{(\rho_{819} + \rho_{1649})^4}$$

Eq. 23

Error in NDII has been calculated for all combinations of ρ_{819} and ρ_{1649} reflectance values from 5% to 95% for 2%, 5%, and 10% error in those values. The surface plot for the 5% error calculations are in **Figure 6**.

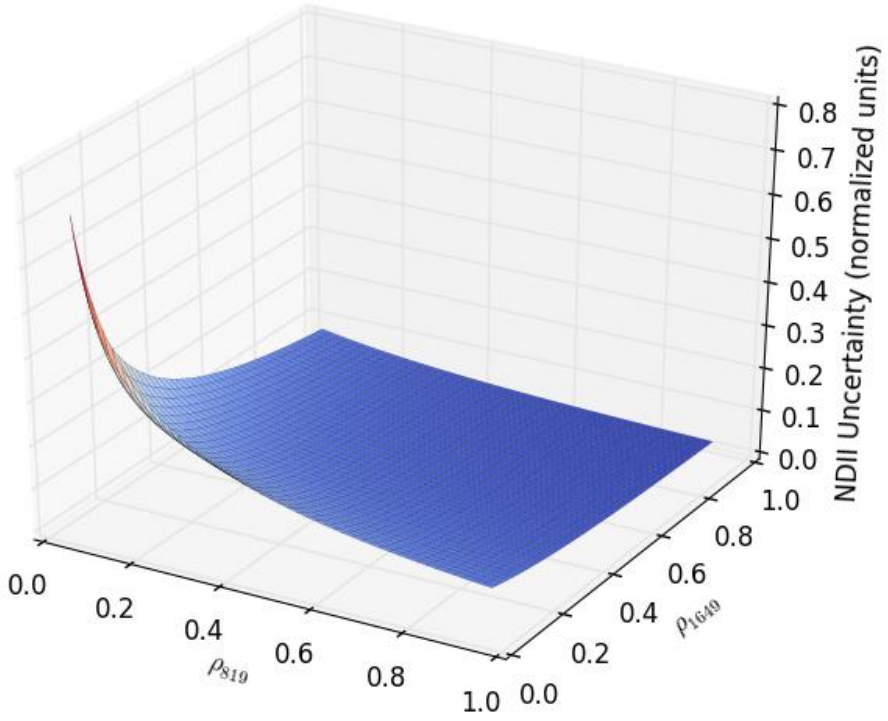

Figure 6. Error in NDII as a function of input reflectance values with 5% uncertainty. Error surfaces for NDII with different reflectance value uncertainty retain the same shape and differ only by magnitude.

6.1.5 MSI Uncertainty

Because MSI is a simple two-band ratio, as shown earlier in Eq. 5, MSI can theoretically range from zero to infinity. The equation for MSI uncertainty as derived from Eq. 7 is shown in Eq. 8 (Huete et al., 1999).

$$u_{cal}^2(MSI) = \left(\frac{\partial MSI}{\partial \rho_{1599}}\right)^2 u_{cal}^2(\rho_{1599}) + \left(\frac{\partial MSI}{\partial \rho_{819}}\right)^2 u_{cal}^2(\rho_{819}) + 2\frac{\partial MSI}{\partial \rho_{1599}}\frac{\partial MSI}{\partial \rho_{819}} u_{cal}(\rho_{1599}, \rho_{819}) \quad \textbf{Eq. 24}$$

where

$$\frac{\partial MSI}{\partial \rho_{1599}} = \frac{1}{\rho_{819}} \quad \textbf{Eq.25}$$

$$\frac{\partial MSI}{\partial \rho_{900}} = -\frac{\rho_{1599}}{{\rho_{819}}^2} \quad \textbf{Eq. 26}$$

$$\frac{\partial MSI}{\partial \rho_{1599}} \frac{\partial MSI}{\partial \rho_{819}} = -\frac{\rho_{1599}}{{\rho_{819}}^3} \quad \textbf{Eq. 27}$$

Error in MSI has been calculated for all combinations of ρ_{1599} and ρ_{819} reflectance values from 5% to 95% for 2%, 5%, and 10% error in those values. The surface plot for the 5% error calculations are in **Figure 7**.

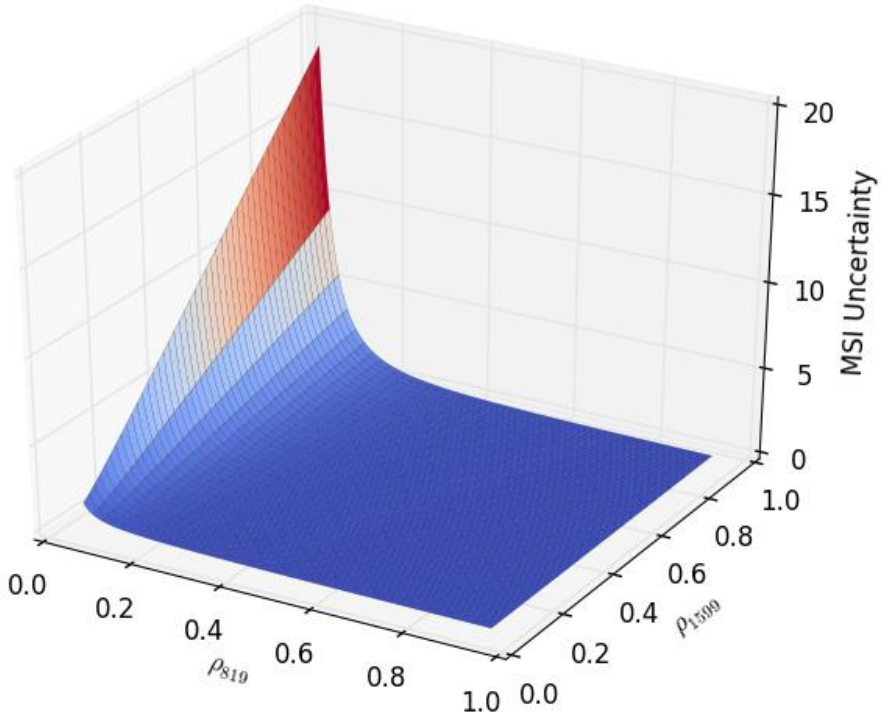

Figure 7. Error in MSI as a function of input reflectance values with 5% uncertainty. Error surfaces for MSI with different reflectance value uncertainty retain the same shape and differ only by magnitude.

6.2 Reported Uncertainty

Currently, no uncertainty is reported with the Canopy Water Content spectral index product. In the future, the uncertainty associated with each pixel will be reported in a separate raster of uncertainty values. The uncertainty will be obtained from the reflectance errors propagated through the appropriate index formulae as was done for the surfaces in 6.1. This form of communicating uncertainty in remote sensing products is consistent with similar spectral index products such as MODIS Vegetation Index Product Series Collection 5. NEON, operating in data acquisition, processing, and distribution roles, has a unique opportunity to create and provide this more detailed information on uncertainty within given data products, such as canopy water content spectral indices, to researchers and end users. This upgrade is planned for implementation in 2018.

7 VALIDATION AND VERIFICATION

7.1 Algorithm Validation

The algorithms as implemented are already defined and agreed upon in the remote sensing disciplines. However, if newer, more preferable indices arise they may be added to the NEON Data Products Catalog, complementing or replacing other canopy water content spectral indices as necessary.

Validation of the algorithm implementation was performed by comparing NEON-produced canopy water content index values to those from the commercial software package ENVI. The validation comparison was run on data from the NEON 2017 collection over the Harvard Forest site (HARV). Differencing the ENVI and NEON canopy water indices showed the results matched to the level of precision offered in the single precision floating point IEEE data type used to store the reflectance data and to perform the calculations.

7.2 Data Product Validation

During observatory operations, canopy water content index products will be validated against similar data products derived from other well-established and calibrated sensor programs such as Landsat. These validation analyses are planned to begin in 2018. NIS imagery will be spatially aggregated and spectrally resampled to match the bandpasses and pixel sizes of candidate validation datasets. Most multispectral sensors do not have the required bands for all NEON canopy water content spectral index products.

7.3 Data Product Verification

During observatory operations, data product verification for canopy water content spectral indices will be accomplished using directly measured field reflectance spectra. NEON AOP operations include periodic acquisition of field spectra during data acquisition flights as a level-of-effort activity. The field spectra will be used to verify L1 directional reflectance products as well as canopy water content spectral index products.

8 FUTURE PLANS AND MODIFICATIONS

A more sophisticated approach for selecting the NIS bands to be used in index calculations is currently in development, similar to that used in making the FPAR data product [RD 06]. The new approach will use a weighted combination of a number of NIS bands to optimally cover the range of the spectral feature of interest. This will result in an implementation of the standard canopy water content spectral index algorithms in a way making them most comparable between sensors, more robust to noise and/or error in individual bands, and better able to properly capture the index value for different types of land cover when the exact location of the spectral feature of interest differs somewhat from the average.

After the band center is mapped to a specific pixel, additional pixels around the central wavelength pixel are co-added and weighted to meet the desired spectral bandpass for the given spectral band. Optimal bandwidths for the bandpasses vary from one spectral index to the next. NIS 5 nm bandpasses allow for very precise targeting of the spectral features required for each index. For narrowband spectral indices, e.g. NDWI, the 5 nm NIS bandpasses meet the standard in research and industry and only 2 or 3 NIS bands may be combined. Broadband indices originally designed for use with data from orbital multispectral sensors such as MODIS and Landsat may use many more NIS bands for recombination. NEON will be implementing combining multiple NIS bands in to bandpasses appropriate for use in these indices in 2018. Early indications are that combining several NIS bands may provide a more robust and cross-sensor compatible product while helping to improve quality (Hulslander et al., 2015).

The modeled, predicted uncertainty ranges in this document will be continuously validated against measured uncertainty in actual NIS data as it is collected. This document will be updated accordingly with the results and plots of those comparisons.

9 BIBLIOGRAPHY

Borengasser, M., Hungate, W.S., & Watkins, R. (2008). *Hyperspectral Remote Sensing*. CRC Press. Boca Raton, FL.

Carlson, K.M., Asner, G.P., Hughes, R.F., Ostertag, R., Martin, R.E. (2007). Hyperspectral Remote Sensing of Canopy Biodiversity in Hawaiian Lowland Rainforests. *Ecosystems, 10*, 536-549.

Chuvieco, E., Riaño, D., Aguado, I., & Cocero, D. (2002). Estimation of fuel moisture content from multitemporal analysis of Landsat Thematic Mapper reflectance data: applications in fire danger assessment. *International Journal of Remote Sensing, 23*(11), 2145-2162.

Clark, R.N., King, T.V.V., Ager, C., & Swayze, G. (1995). "Initial Vegetation Species and Senescence/Stress Indicator Mapping in the San Luis Valley, Colorado Using Imaging Spectrometer Data". Proceedings of Summitville Forum '95. Posey, H.H., J.A. Pendleton, D. Van Zyl (eds.). *Colorado Geological Survey Special Publication, 38*, 64-69.

Coops, N.C., Johnson, M., Wulder, M.A., & White, J.C. (2006). Assessment of QuickBird high spatial resolution imagery to detect red attack damage due to mountain pine beetle infestation. *Remote Sensing of Environment, 103*, 67-80.

Dasgupta, S., Qu, J.J., Hao, X., & Bhoi, S. (2007). Evaluating remotely sensed live fuel moisture estimations for fire behavior predictions in Georgia, USA. *Remote Sensing of Environment, 108*, 138-150.

Foley, J.A., Prentice, C.I., Ramankutty, N., Levis, S., Pollard, D. Sitch, S., & Haxeltine, A. (1996). An integrate biosphere model of land surface processes, terrestrial carbon balance, and vegetation dynamics. *Global Biogeochemical Cycles, 10*(4), 603-628.

Gao, B.-C. (1996). NDWI – A Normalized Difference Water Index for Remote Sensing of Vegetation Liquid Water from Space. *Remote Sensing of Environment, 58*, 257-266.

Govender, M., Chetty, K., & Bulcock, H. (2007). A review of hyperspectral remote sensing and its application in vegetation and water resource studies. *Water SA, 33*(2), 145-152.

Hardisky, M.A., Klemas, V., & Smart, R.M. (1983). The Influence of Soil Salinity, Growth Form, and Leaf Moisture on the Spectral Radiance of *Spartina alterniflora* Canopies. *Photogrammetric Engineering and Remote Sensing, 49*(1), 77-83.

Huete, A., Justice, C., & Van Leeuwen, W. (1999). MODIS vegetation index (MOD13). *Algorithm Theoretical Basis Document*, *3*, 213.

Hulslander, D., Kampe, T., Goulden, T., Krause, K., Leisso, N., Gallery, W. (2015). Quantitative Determination of Bandpasses for Producing Vegetation Indices from Recombined NEON Hyperspectral Imagery. Abstract B53F-0632 presented at 2015 Fall Meeting, AGU, San Francisco, CA, 14-18 Dec.

Hunt, E.R. & Rock, B.N. (1989). Detection of Changes in Leaf Water Content Using Near- and Middle-Infrared Reflectances. *Remote Sensing of Environment, 30*, 43-54.

Jackson, T.J., Chen, D., Cosh, M., Li, F., Anderson, M., Walthall, C., Doriaswamy, P., & Hunt, E.R. (2003). Vegetation water content mapping using Landsat data derived normalized difference water index for corn and soybeans. *Remote Sensing of Environment, 92*, 475-482.

Jones, J. G. & Vaughan, R. A. (2010). *Remote Sensing Of Vegetation*. Oxford University Press. New York, NY.

Miura, T., Huete, A. R., & Yoshioka, H. (1999). Evaluation of sensor calibration uncertainties on vegetation indices for MODIS. submitted to *IEEE Trans. Geosci. Remote Sens.*.

Nagler, P.L., Glenn, E.P., Kim, H., Emmerich, W., Scott, R.L., Huxman, T.E., & Huete, A.R. (2007). Relationship between evapotranspiration and precipitation pulses in a semiarid rangeland estimated by moisture flux towers and MODIS vegetation indices. *Journal of Arid Environments, 70*, 443-462.

National Research Council. (2001). Grand Challenges in Environmental Sciences. Washington, DC: National Academies Press.

NCSL. (1997). American National Standard for Expressing Uncertainty – U.S. Guide to the Expression of Uncertainty in Measurement, ANSI/NCSL Z540-2-1997, *National Conference of Standards Laboratories (NCSL)*, Boulder, CO, 101p.

NEON. (2011). 2011 Science Strategy Enabling Continental-Scale Ecological Forecasting. Boulder, CO. http://www.neonscience.org/sites/default/files/basic-page-files/NEON_Strategy_2011u2_0.pdf

Ortenberg, F. (2012). Hyperspectral Sensor Characteristics: Airborne, Spaceborne, Hand-Held, and Truck-Mounted; Integration of Hyperspectral Data with LIDAR. *Hyperspectral Remote Sensing of Vegetation*. Taylor and Francis Group.

Peñuelas, J., Filella, I., Biel, C., Serrano, L., & Savé, R. (1993). The reflectance at the 950-970 nm region as an indicator of plant water status. *International Journal of Remote Sensing, 14*(10), 1887-1905.

Roberts, D. A., Roth, K. L., & Perroy, R. L. (2016). 14 Hyperspectral Vegetation Indices. *Hyperspectral Remote Sensing of Vegetation, 309*.

Rock, B.N., Williams, D.L., & Vogelmann, J.E. (1985). Field and airborne spectral characterization of suspected acid deposition damage in red spruce (*Picea rubens*) from Vermont. *Proceedings of the 11th International Symposium on Machine Processing of Remotely Sensed Data*. Purdue University, West Lafayette, IN.

Rock, B.N., Vogelmann, J.E., Williams, D.L., Vogelmann, A.F., & Hoshizaki, T. (1986). Remote Detection of Forest Damage. *Bioscience, 36*(7), 439-445.

Rodriguez-Iturbe, I. (2000). Ecohydrology: A hydrologic perspective of climate-soil-vegetation dynamics. *Water Resources Research, 36*(1), 3-9.

Scanlon, B.R., Reedy, R.C., Stonestrom, D.A., Prudic, D.E., & Dennehy, K.F. (2005). Impact of land use and land cover change on groundwater recharge and quality in the southwestern US. *Global Change Biology, 11*(10), 1577-1593.

Schlesinger, W.H. & Bernhardt, E.S. (2013). *Biogeochemistry, An Analysis of Global Change*. Elsevier.

Short, N.M. (1982). "The LANDSAT Tutorial Workbook: Basics of Satellite Remote Sensing". NASA Reference Publication 1078. NASA.

Skakun, R.S., Wulder, M.A., & Franklin, S.E. (2003). Sensitivity of the thematic mapper wetness difference index to detect mountain pine beetle red-attack damage. *Remote Sensing of Environment, 86*, 433-443.

Sriwongsitanon, N., Gao, H., Savenije, H.H.G., Maekan, E., Saengsawang, S., & Thianpopirug, S. (2015). The Normalized Difference Infrared Index (NDII) as a proxy for soil moisture storage in hydrological modelling. *Hydrology and Earth System Sciences Discussions, 12*, 8419-8457.

Taylor, B. N. & Kuyatt, C. E. (1994). Guidelines for Evaluating and Expressing the Uncertainty of NIST Measurement Results. *NIST Technical Note 1297*, 1994 Ed., Gaithersburg, MD, 24p.

Thenkabail, P. S., Lyon, J. G., & Huete, A. (2012). *Hyperspectral Remote Sensing of Vegetation*. Taylor and Francis Group.

USGS, (2013). How does Landsat 8 differ from previous Landsat satellites?. Reston, VA. Available online at http://landsat.usgs.gov/ldcm_vs_previous.php

van der Meer, F.D. & de Jong, S.M. (2011). *Imaging Spectrometry*. Springer. Dordrecht, The Netherlands.

Vane, G. (1987). Airborne Visible/Infrared Imaging Spectrometer (AVIRIS). In *Imaging Spectroscopy II Conference of the 31st Annual International Symposium on Optical and Optoelectronic Applied Science and Engineering, San Diego, CA*.

Wang, L. & Qu, J.J. (2007). NMDI: A normalized multi-band drought index for monitoring soil and vegetation moisture with satellite remote sensing. *Geophysical Research Letters, 34*. L20405. 10.1029/2007GL031021.

Wang, L., Qu, J.J., Hao, X. (2008). Forest fire detection using the normalized multi-band drought index (NMDI) with satellite measurements. *Agricultural and Forest Meteorology, 148*, 1767-1776.

Wilcox, B.P. & Thurow, T.L. (2006). Emerging Issues in Rangeland Ecohydrology: Vegetation Change and the Water Cycle. *Rangeland Ecology & Management, 59*(2), 220-224.